

Improving Inferences about Exoplanet Habitability [†]

Risinie D. Perera  and Kevin H. Knuth * 

Physics Department, University at Albany (SUNY), Albany, NY 12222, USA; rperera@albany.edu

* Correspondence: kknuth@albany.edu

† Presented at the 42nd International Workshop on Bayesian Inference and Maximum Entropy Methods in Science and Engineering, Garching, Germany, 3–7 July 2023.

Abstract: Assessing the habitability of exoplanets (planets orbiting other stars) is of great importance in deciding which planets warrant further careful study. Planets in the habitable zones of stars like our Sun are sufficiently far away from the star so that the light rays from the star can be assumed to be parallel, leading to straightforward analytic models for stellar illumination of the planet's surface. However, for planets in the close-in habitable zones of dim red dwarf stars, such as the potentially habitable planet orbiting our nearest stellar neighbor, Proxima Centauri, the analytic illumination models based on the parallel ray approximation do not hold, resulting in severe biases in the estimates of the planetary characteristics, thus impacting efforts to understand the planet's atmosphere and climate. In this paper, we present our efforts to improve the instellation (stellar illumination) models for close-in orbiting planets and the significance of the implementation of these improved models into EXONEST, which is a Bayesian machine learning application for exoplanet characterization. The ultimate goal is to use these improved models and parameter estimates to model the climates of close-in orbiting exoplanets using planetary General Circulation Models (GCM). More specifically, we are working to apply our instellation corrections to the NASA ROCKE-3D GCM to study the climates of the potentially habitable planets in the Trappist-1 system.

Keywords: exoplanet characterization; Bayesian inference; EXONEST; ROCKE-3D GCM; General Circulation Models; astrophysics; instellation; Trappist-1



Citation: Perera, R.D.; Knuth, K.H. Improving Inferences about Exoplanet Habitability. *Phys. Sci. Forum* **2023**, *9*, 7. <https://doi.org/10.3390/psf2023009007>

Academic Editors: Udo von Toussaint and Roland Preuss

Published: 27 November 2023



Copyright: © 2023 by the authors. Licensee MDPI, Basel, Switzerland. This article is an open access article distributed under the terms and conditions of the Creative Commons Attribution (CC BY) license (<https://creativecommons.org/licenses/by/4.0/>).

1. Introduction

Typically, the illumination of exoplanets is determined under the assumption that the incident stellar radiation reaches the exoplanet as plane parallel rays. In this situation, half of the planet is fully illuminated and the other half is dark. For extremely close-in exoplanets for which the star-planet separation is on the order of only a few stellar radii, it is particularly important to take into account the finite angular size of the host star. Doing so reveals that two additional zones are necessary to describe the illumination of the exoplanet. Previous work has shown that the planet will have four distinct illumination zones: the fully-illuminated zone, the first penumbral zone, the second penumbral zone, and the un-illuminated (or night) zone [1] (Figure 1).

The fully-illuminated zone (FZ) is the region on the planet in which the entire apparent disk of the star is visible in the sky. However, due to the close-in geometry, the surface area of the visible star is less than one-half of the total area. The first penumbral zone (PZ_1) is the region on the planet in which a portion of the star (less than one-half of the potentially visible area) is occluded by the horizon; that is, the star is on the verge of setting. The second penumbral zone (PZ_2) is the region on the planet in which more than one-half of the potentially visible area of the star is occluded by the horizon and the un-illuminated zone (UZ) is the region on the planet from which the star cannot be seen.

The result is that the rather abrupt terminator between the day-side and night-side of a distant planet is, in the case of a close-in planet, spread out into the two penumbral zones, which impinge on both the fully illuminated and the un-illuminated zones. So while a

smaller surface area of the close-in planet is fully-illuminated, more of the planet’s surface receives light because the un-illuminated zone is also smaller. For example, in the case of the close-in orbiting hot Jupiter, Kepler-91b, about 30% of the surface is in full daylight, 40% of the surface is in partial penumbral light, and 30% of the surface is in full darkness, so that approximately 70% of the planet is receiving some light at any point in time [2]. These differences in illumination are expected to impact the planet’s climate.

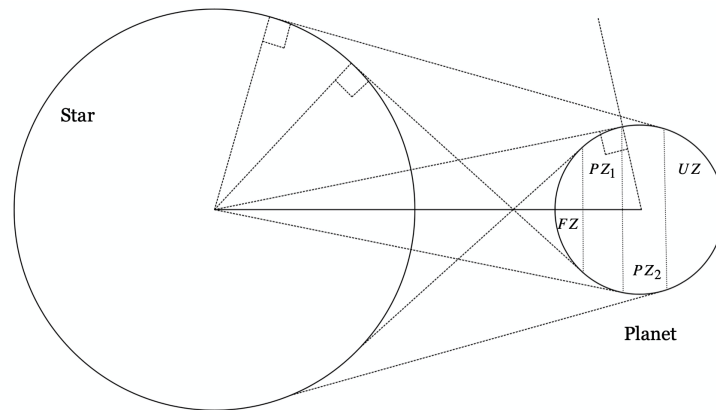


Figure 1. Extremely close-in exoplanets exhibit four zones of illumination: a fully illuminated zone (FZ) defined by the inner tangents, two penumbral zones (PZ₁, PZ₂) defined by whether more than half or less than half of the star is visible, and a dark un-illuminated zone (UZ) defined by the outer tangents.

The main goal of this paper is to construct analytic expressions for the flux incident on an exoplanet to be implemented in EXONEST, a Bayesian machine learning application developed for exoplanet characterization [2,3].

2. Methods

In this section we build analytic expressions for the light received by a point on the exoplanet taking into account the finite angular size of the host star.

2.1. Instellation Setup

Suppose that the star emits P photons per unit time. Integrating the photons over the blackbody spectrum will give the amount of emitted energy, and therefore this P is related to the power emitted by the star. If each area element of the star, $d\sigma_s$, emits dp photons per unit time, the total number of photons emitted by the star in unit time, P , is given by:

$$P = \int dp. \tag{1}$$

If p is the number of photons emitted by an area element in a unit time, then

$$dp = p d\sigma_s, \tag{2}$$

and

$$P = \iint p d\sigma_s. \tag{3}$$

Let the radius of the star be R_s . Assuming the star to be a sphere, we can write $d\sigma_s$ in terms of the surface area element as

$$P = \iint p R_s^2 \sin \theta d\theta d\omega. \tag{4}$$

Integrating over the whole star yields

$$P = p(4\pi R_S^2), \tag{5}$$

which allows us to write

$$p = \frac{P}{4\pi R_S^2}. \tag{6}$$

Some of these photons will hit the planet.

Next, let us consider photons emitted from the area element on the stellar surface at point *A*, and determine how many of these photons will be incident at a point *B* on the planet. Let $df_{A \rightarrow B}$ denote the number of photons emitted by *A* and arriving at *B* in a unit time. Then, from Figure 2:

$$df_{A \rightarrow B} = \left[\frac{(\hat{m} \cdot \hat{\rho}')(\hat{n} \cdot \hat{\rho}')}{\rho'^2} \right] dp. \tag{7}$$

Substituting $\hat{\rho}' = \frac{\vec{\rho}'}{\rho'}$ and dp using Equations (2)–(6) gives:

$$df_{A \rightarrow B} = -\frac{P}{4\pi} \left[\frac{(\hat{m} \cdot \vec{\rho}')(\hat{n} \cdot \vec{\rho}')}{\rho'^4} \right] \sin \theta d\theta d\omega. \tag{8}$$

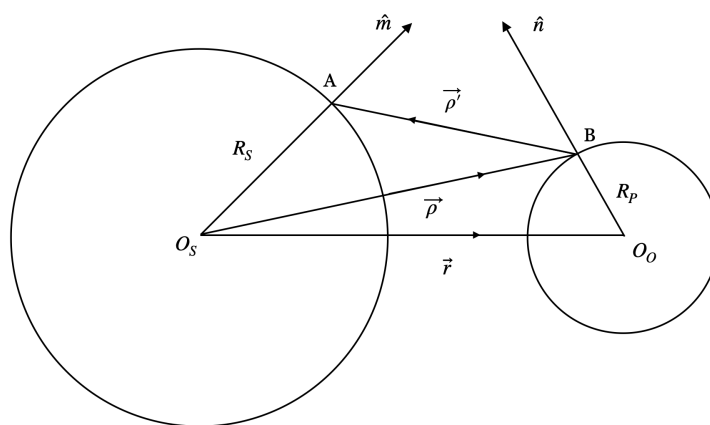


Figure 2. Star–planet geometry involving light emission at point *A* on the star and incident on the planet at point *B*: The star with radius R_S is centered at O_S and the exoplanet with radius R_P is centered at O_O . The star–planet separation is denoted by the vector \vec{r} .

2.2. Coordinate Systems

When we have a star–planet dynamical system, it is convenient to introduce three coordinate systems: stellar, planetocentric, and overall. For the scope of this paper, it suffices to use just two, stellar and overall, by choosing the origin of the overall coordinate system at the center of the exoplanet such that it would coincide with the planetocentric coordinate system (Figure 3). Furthermore, the axial symmetry of stellar illumination about the axis joining the centers of the planet and the star can be exploited by orienting the *z*-axis of the overall coordinate system in this direction. With this coordinate system, the problem simplifies to having to determine the illumination along one semicircular arc.

The stellar and overall Cartesian coordinate systems are related to one another as follows:

$$(x_o, y_o, z_o)_o = (-x_o, y_o, r - z_o)_s \tag{9}$$

and

$$(x_s, y_s, z_s)_s = (-x_s, y_s, r - z_s)_o. \tag{10}$$

Now that we have chosen appropriate coordinate systems, next let us derive the vectors required for the illumination in (8).

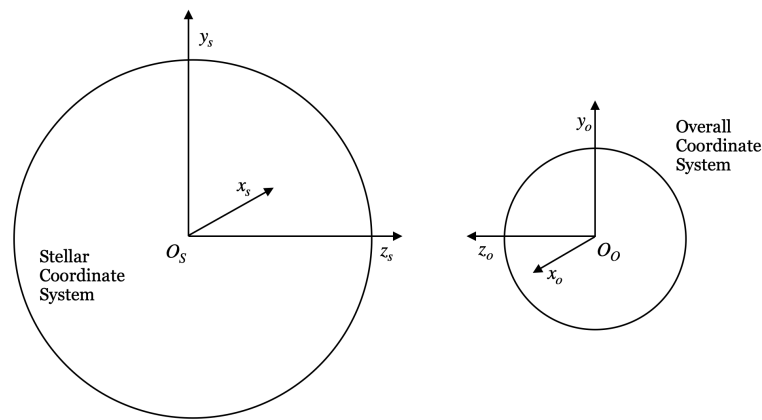


Figure 3. Orientations of the stellar and overall coordinate systems with origins located at O_S and O_O , respectively. The stellar coordinate system, which employs spherical coordinates (θ, ω) , is used to define points on the star, while the overall coordinate system employs spherical coordinates (η, ϕ) .

2.3. The Vector $\vec{\rho}$

The vector $\vec{\rho}$ is given by

$$\vec{\rho} = \vec{r} + \overrightarrow{O_P B}, \tag{11}$$

where in the overall frame

$$\vec{r} = -r \hat{z}_o, \tag{12}$$

and $\overrightarrow{O_P B}$ is the position vector of the point B in the overall frame:

$$\overrightarrow{O_P B} = R_P \sin \eta \cos \phi \hat{x}_o + R_P \sin \eta \sin \phi \hat{y}_o + R_P \cos \eta \hat{z}_o. \tag{13}$$

The sum then gives

$$\vec{\rho} = R_P \sin \eta \cos \phi \hat{x}_o + R_P \sin \eta \sin \phi \hat{y}_o + (R_P \cos \eta - r) \hat{z}_o, \tag{14}$$

which has a magnitude of

$$\rho = \left(r^2 - 2rR_P \cos \eta + R_P^2 \right)^{1/2}. \tag{15}$$

We can now verify that if the point B is located at $(\eta, \phi) = (0, \pi/2)$, then

$$\rho(\eta = 0, \phi = \pi/2) = \left(r^2 - 2rR_P + R_P^2 \right)^{1/2} = r - R_P, \tag{16}$$

as expected.

2.4. The Vector $\vec{\rho}'$

Let us consider the triangle $O_S A B$ in Figure 2.

$$\overrightarrow{B A} = \overrightarrow{B O_S} + \overrightarrow{O_S A}, \tag{17}$$

$$\vec{\rho}' = -\vec{\rho} + \overrightarrow{O_S A}. \tag{18}$$

The vector $\overrightarrow{O_S A}$ in the stellar coordinate system is given by

$$\overrightarrow{O_S A} = R_S \sin \theta \cos \omega \hat{x}_s + R_S \sin \theta \sin \omega \hat{y}_s + R_S \cos \theta \hat{z}_s. \tag{19}$$

Constructing the vector $\overrightarrow{O_S A}$ in the overall coordinate system requires some care. We can use the fact that

$$\overrightarrow{O_S A} = \overrightarrow{O_S O_O} + \overrightarrow{O_O A}, \tag{20}$$

where by the relation in Equation (10),

$$\overrightarrow{O_O A} = -R_S \sin \theta \cos \omega \hat{x}_o + R_S \sin \theta \sin \omega \hat{y}_o + (r - R_S \cos \theta) \hat{z}_o \tag{21}$$

and

$$\overrightarrow{O_S O_O} = -r \hat{z}_o, \tag{22}$$

such that

$$\overrightarrow{O_S A} = -R_S \sin \theta \cos \omega \hat{x}_o + R_S \sin \theta \sin \omega \hat{y}_o - R_S \cos \theta \hat{z}_o, \tag{23}$$

which simplifies to

$$\begin{aligned} \vec{\rho}' = & -(R_P \sin \eta \cos \phi + R_S \sin \theta \cos \omega) \hat{x}_o \\ & - (R_P \sin \eta \sin \phi - R_S \sin \theta \sin \omega) \hat{y}_o \\ & + (r - R_P \cos \eta - R_S \cos \theta) \hat{z}_o. \end{aligned} \tag{24}$$

The squared-magnitude of ρ' is

$$\begin{aligned} \rho'^2 = & R_P^2 + R_S^2 + r^2 - 2r(R_P \cos \eta + R_S \cos \theta) + \\ & 2R_P R_S (\sin \eta \cos \phi \sin \theta \cos \omega + \cos \eta \cos \theta - \sin \eta \sin \phi \sin \theta \sin \omega). \end{aligned} \tag{25}$$

The distance ρ' is then found by taking the square root of the result above.

We can check this result by looking at points $B = (\eta = 0, \phi = \pi/2)$ and $A = (\theta = 0, \omega = 0)$ for which

$$\rho'^2 = R_P^2 + R_S^2 + r^2 - 2r(R_P + R_S) + 2R_P R_S, \tag{26}$$

such that

$$\rho' = r - (R_P + R_S), \tag{27}$$

as expected.

2.5. The Unit Vectors

Now let us obtain the relevant unit vectors, \hat{m} and \hat{n} , in the overall coordinate system. Note that \hat{m} is the unit vector in the $\overrightarrow{O_S A}$ direction and therefore

$$\hat{m} = \frac{\overrightarrow{O_S A}}{|\overrightarrow{O_S A}|}. \tag{28}$$

Noting that $|\overrightarrow{O_S A}| = R_S$, by Equation (23) we have

$$\hat{m} = -\sin \theta \cos \omega \hat{x}_o + \sin \theta \sin \omega \hat{y}_o - \cos \theta \hat{z}_o. \tag{29}$$

Similarly noting that \hat{n} is the unit vector in the $\overrightarrow{O_P B}$ direction and using Equation (13) gives

$$\hat{n} = \sin \eta \cos \phi \hat{x}_o + \sin \eta \sin \phi \hat{y}_o + \cos \eta \hat{z}_o. \tag{30}$$

With an understanding of how to construct the relevant vectors and express them in the overall coordinate system, we can now write out the necessary integrals to obtain the total instellation.

2.6. Total Instellation

To compute the total instellation, we must integrate over the visible surface of the star, which is described by the spherical coordinates θ and ω . The total instellation at a point B on the planet is given by integrating over all possible points, A , on the star that is visible to point B on the planet:

$$f_B = - \int_{\omega_1}^{\omega_2} \int_{\theta_1}^{\theta_2} \frac{P}{4\pi} \left[\frac{(\hat{m} \cdot \vec{\rho}')(\hat{n} \cdot \vec{\rho}')}{\rho'^4} \right] \sin \theta d\theta d\omega \quad (31)$$

where $\theta_1, \theta_2, \omega_1$ and ω_2 are the limits of integration that depend on the zone in which point B is located.

Upon substitution of $\vec{\rho}'$, its magnitude and the unit vectors \hat{m} and \hat{n} , into the total instellation in (31), it simplifies to 5 distinct double integrals with respect to θ and ω , which must be integrated over the limits of each zone to obtain an analytic model.

3. Discussion

In this section, we discuss the applications and implications of improved instellation models to illustrate the benefits of having accurate models for stellar illumination in order to determine the habitability of close-in exoplanets.

3.1. Bayesian Exoplanet Characterization and Model Testing

The EXONEST software suite performs Bayesian model-based exoplanet characterization using photometric and radial velocity data [2–5]. EXONEST relies on predictive photometric models that generate a predicted stellar light curve based on a set of hypothesized model parameters. Bayesian probability theory [6–9] uses this predicted stellar light curve to compute the posterior probability that the set of hypothetical model parameters could have been responsible for the recorded light curve. This allows detailed astrophysical models to be evaluated by the data analysis algorithm, as well as statistical testing among competing models [3,8,10,11]. EXONEST allows the user to employ one of several variants of the Nested Sampling Algorithm, such as Nested Sampling [8,12], Multi-Nest [13,14], and the state-of-the-art Nested Sampling with Galilean Monte Carlo [15–17]. These Nested Sampling algorithms provide estimates of the model parameter values as well as the Bayesian evidence, which allows for statistical model testing. Using evidence-based Bayesian techniques [10], exoplanetary models can be ranked based on the Bayesian evidence providing the capability for scientific hypothesis testing. One can test various photometric effects and compute the evidence to determine the probability that these effects are present in any given system. Relying on data from the NASA Exoplanet Archive, we can utilize EXONEST and its ability to perform Bayesian model testing to evaluate the efficacy of our improved instellation models by computing the Bayesian evidence of the parallel-ray approximation models versus our proposed models.

In any problem involving model parameter estimation, there are legitimate concerns about potential degeneracies among the model parameters, especially as the number of parameters increases. Degeneracies can be expected when more than one parameter affects the predicted light curve in a similar way. In reality, this is a warning that additional, different data are needed to effectively estimate the model parameters. Examining the cross-correlations between the parameter estimates is a very effective way to identify degeneracies. Model testing, as described above, can be used to detect degeneracies as well, since a degenerate set of model parameters will not significantly increase the likelihood function, but it will significantly decrease the prior probability, resulting in lower evidence.

3.2. Implications for Potentially Habitable M-Dwarf Worlds

The exoplanet TRAPPIST-1d ($R_{star} = 0.00056 \text{ AU} = 0.121R_{SUN}$, $a = 0.022 \text{ AU} = 39R_{star}$), which closely orbits its host M-dwarf star in the habitable zone (HZ), has a penumbral zone that covers about 2.5% of its surface or 8.25 million km^2 . While this is a small percentage of the surface of the planet, this is greater than the area of Central and South America combined, which contains several important biogeographical regions on Earth. (e.g., [18–21]). Our estimates reveal that planets orbiting M-dwarf stars on the inner edge of the HZ will have penumbral zones ranging in area from around 1 to 3% of the surface area of the planet. While this may seem like a small value, it may have its greatest climatological impact at the poles of low obliquity worlds where the ice–albedo feedback manifests itself consistently and tends to drive mean surface temperatures lower, which can affect the fractional habitability metrics like that proposed in [22]. A detailed understanding of the incident stellar radiation in these penumbral regions is expected to have significant relevance to understanding habitability on these worlds.

3.3. Climate Modeling of Close-In Orbiting Planets

As mentioned before, corrections are required to the illumination models used in planetary General Circulation Models (GCM) in order to properly model the climate of a close-in exoplanet. The analytical expressions for the incident stellar flux can be applied to the illumination model in the ROCKE-3D GCM [23]. Not only have such corrections never been applied in a GCM, but their effects have never been quantified. For example, differences in illumination at the poles of zero obliquity worlds due to these corrected illumination models could have large effects on ice coverage at the poles. Recent work [24] has shown that polar supercontinents and ocean circulation can affect global mean surface temperatures by several degrees because of the extent of polar ice and the resulting ice–albedo feedback. We expect corrected illumination models to have similar effects. Using the modified ROCKE-3D code for close-in planets, we could study the climates of potentially habitable planets. Critically, we can make one-to-one comparisons of GCM results between penumbral and parallel ray (the current default) illuminations and derive statistical measures of difference (e.g., systematic latitudinal—and global—surface temperature differences, ice-cover, precipitation patterns). We could look at a variety of topographies, land/sea masks, and surface water content used in previous ROCKE-3D publications such as Proxima Centauri b [25], Future Earth [24], and ancient Venus [26].

4. Conclusions

Developing accurate analytical stellar instellation models for close-in orbiting exoplanets will increase both the accuracy and precision of inferred model parameter estimates obtained from data, thereby improving exoplanet characterization and potentially the detection of habitable exoplanets. This is a multidisciplinary project, founded on astrophysics with machine learning. Studying the implications of these improved illumination models in the context of exoplanetary climate modeling will provide a better understanding of the climates and atmospheric physics of close-in orbiting exoplanets.

Author Contributions: The authors contributed equally to the project. All authors have read and agreed to the published version of the manuscript.

Funding: This research received no external funding.

Institutional Review Board Statement: Not applicable.

Informed Consent Statement: Not applicable.

Data Availability Statement: Data sharing is not applicable to this article.

Acknowledgments: We wish to thank Jennifer L. Carter, Michael J. Way, Oleg Lunin and Jonathan Petrucci for helpful advice as well as the organizers, Udo von Toussaint, Roland Preuss, Svenja Eichler and Anja Bauer for their generous hospitality.

Conflicts of Interest: The authors declare no conflict of interest.

References

1. Carter, J.L. *Estimation of Planetary Photometric Emissions for Extremely Close-in Exoplanets*; University at Albany: Albany, NY, USA, 2018.
2. Knuth, K.H.; Placek, B.; Angerhausen, D.; Carter, J.L.; D'Angelo, B.; Gai, A.D.; Carado, B. Exonest: The bayesian exoplanetary explorer. *Entropy* **2017**, *19*, 559. [[CrossRef](#)]
3. Placek, B.; Knuth, K.H.; Angerhausen, D. EXONEST: Bayesian model selection applied to the detection and characterization of exoplanets via photometric variations. *Astrophys. J.* **2014**, *795*, 112. [[CrossRef](#)]
4. Placek, B. *Bayesian Detection and Characterization of Extra-Solar Planets via Photometric Variations*; University at Albany: Albany, NY, USA, 2014.
5. Placek, B.; Knuth, K.H.; Angerhausen, D.; Jenkins, J.M. Characterization of Kepler-91b and the investigation of a potential Trojan companion using EXONEST. *Astrophys. J.* **2015**, *814*, 147. [[CrossRef](#)]
6. Jaynes, E.T. *Probability Theory: The Logic of Science*; Cambridge University Press: Cambridge, UK, 2003.
7. Gregory, P. *Bayesian Logical Data Analysis for the Physical Sciences: A Comparative Approach with Mathematica® Support*; Cambridge University Press: Cambridge, UK, 2005.
8. Sivia, D.; Skilling, J. *Data Analysis: A Bayesian Tutorial*; OUP Oxford: Oxford, UK, 2006.
9. Knuth, K.H.; Skilling, J. Foundations of inference. *Axioms* **2012**, *1*, 38–73. [[CrossRef](#)]
10. Knuth, K.H.; Habeck, M.; Malakar, N.K.; Mubeen, A.M.; Placek, B. Bayesian evidence and model selection. *Digit. Signal Process.* **2015**, *47*, 50–67. [[CrossRef](#)]
11. Gai, A.D.; Knuth, K.H. Bayesian model testing of ellipsoidal variations on stars due to hot Jupiters. *Astrophys. J.* **2018**, *853*, 49. [[CrossRef](#)]
12. Skilling, J. Nested sampling. *AIP Conf. Proc.* **2004**, *735*, 395–405.
13. Feroz, F.; Hobson, M.P. Multimodal nested sampling: An efficient and robust alternative to Markov Chain Monte Carlo methods for astronomical data analyses. *Mon. Not. R. Astron. Soc.* **2008**, *384*, 449–463. [[CrossRef](#)]
14. Feroz, F.; Hobson, M.; Bridges, M. MultiNest: An efficient and robust Bayesian inference tool for cosmology and particle physics. *Mon. Not. R. Astron. Soc.* **2009**, *398*, 1601–1614. [[CrossRef](#)]
15. Skilling, J. Bayesian computation in big spaces-nested sampling and Galilean Monte Carlo. *AIP Conf. Proc.* **2012**, *1443*, 145–156.
16. Feroz, F.; Skilling, J. Exploring multi-modal distributions with nested sampling. *AIP Conf. Proc.* **2013**, *1553*, 106–113.
17. Skilling, J. Galilean and Hamiltonian Monte Carlo. *Multidiscip. Digit. Publ. Inst. Proc.* **2019**, *33*, 19.
18. Dickinson, R.E.; Kennedy, P. Impacts on regional climate of Amazon deforestation. *Geophys. Res. Lett.* **1992**, *19*, 1947–1950. [[CrossRef](#)]
19. Yang, Y.; Saatchi, S.S.; Xu, L.; Yu, Y.; Choi, S.; Phillips, N.; Kennedy, R.; Keller, M.; Knyazikhin, Y.; Myneni, R.B. Post-drought decline of the Amazon carbon sink. *Nat. Commun.* **2018**, *9*, 3172. [[CrossRef](#)] [[PubMed](#)]
20. Molina, R.; Salazar, J.; Martínez, J.; Villegas, J.; Arias, P. Exponential growth of precipitation along a “forest-fed moisture convey or belt” above the Amazon. *J. Geophys. Res. Atmos* **2019**, *124*, 2589–2599. [[CrossRef](#)]
21. Pereira, J.C. Reducing catastrophic climate risk by revolutionizing the Amazon: Novel pathways for Brazilian diplomacy. In *Climate Change and Global Development: Market, Global Players and Empirical Evidence*; Springer: Berlin/Heidelberg, Germany, 2019; pp. 189–218.
22. Spiegel, D.S.; Menou, K.; Scharf, C.A. Habitable climates. *Astrophys. J.* **2008**, *681*, 1609. [[CrossRef](#)]
23. Way, M.J.; Aleinov, I.; Amundsen, D.S.; Chandler, M.; Clune, T.; Del Genio, A.D.; Fujii, Y.; Kelley, M.; Kiang, N.Y.; Sohl, L.; et al. Resolving orbital and climate keys of Earth and extraterrestrial environments with dynamics (ROCKE-3D) 1.0: A general circulation model for simulating the climates of rocky planets. *Astrophys. J. Suppl. Ser.* **2017**, *231*, 12. [[CrossRef](#)]
24. Way, M.J.; Davies, H.S.; Duarte, J.C.; Green, J. The climates of Earth's next supercontinent: Effects of tectonics, rotation rate, and insolation. *Geochem. Geophys. Geosyst.* **2021**, *22*, e2021GC009983. [[CrossRef](#)]
25. Del Genio, A.D.; Way, M.J.; Amundsen, D.S.; Aleinov, I.; Kelley, M.; Kiang, N.Y.; Clune, T.L. Habitable climate scenarios for Proxima Centauri b with a dynamic ocean. *Astrobiology* **2019**, *19*, 99–125. [[CrossRef](#)] [[PubMed](#)]
26. Way, M.J.; Del Genio, A.D. Venusian habitable climate scenarios: Modeling Venus through time and applications to slowly rotating Venus-like exoplanets. *J. Geophys. Res. Planets* **2020**, *125*, e2019JE006276. [[CrossRef](#)]

Disclaimer/Publisher's Note: The statements, opinions and data contained in all publications are solely those of the individual author(s) and contributor(s) and not of MDPI and/or the editor(s). MDPI and/or the editor(s) disclaim responsibility for any injury to people or property resulting from any ideas, methods, instructions or products referred to in the content.